Structure and Function in the Isolated Reaction-Center Complex of Photosystem II. 2. Models for Energy Relaxation and Charge Separation in a Protein Matrix

Joseph J. Shiang, Laurie M. Yoder, and Roseanne J. Sension*

Department of Chemistry, University of Michigan, Ann Arbor, Michigan 48109-1055

Received: August 29, 2002

We have developed a model that describes the energy and charge transfer in photosystem II reaction-center complexes, using parameters with clear physical interpretations. The input parameters are deduced from independent experimental work and from the theoretical constraints of the system. This model is comprised of exitonically coupled chlorophyll electronic states, including charge-transfer states, which are coupled to the protein bath. The dynamics of the system are calculated using a master-equation approach, and the results are converted into spectroscopic observables for comparison with experimental data. The model accurately depicts the emission kinetics observed for both bacterial reaction centers from *Rhodobacter sphaeroides* and photosystem II from spinach. The model is discussed with regard to the wavelength dependence of energy transfer, the effects of static disorder in the system, and the initial ultrafast dynamics of the charge separation.

I. Introduction

Photosynthesis in higher plants is one of the key chemical transformations that supports life on earth. The elucidation of the various physical and biological processes that give rise to this particular light-driven chemistry has been the subject of diverse studies involving many different disciplines. The photoconversion process proceeds in several steps involving a variety of distinct protein complexes. The protein complex known as photosystem II (PSII) performs the initial reaction in oxygenic photosynthesis: the conversion of light into a redox pair capable of oxidizing water. In the present paper, we will focus on the initial, or primary, energy-transfer and electron-transfer processes that occur within the PSII reaction center following the absorption of a photon. These picosecond processes have been the subject of a number of detailed optical studies.[1−10] To date however, there has been no firm consensus on the nature and mechanism of the primary charge-separation process.

The optical data obtained from PSII complexes isolated from higher plants are difficult to interpret on a qualitative or quantitative level. There are several reasons for this. First, the electronic energy levels of the chlorophyll and pheophytin pigments contained in the PSII reaction center and the primary charge-separated states are all relatively close to each other, with the absorption and emission bands of the pigments strongly overlapping. Second, while a structure of the PSII reaction center has been reported recently,[11] the resolution is not sufficient to specify the exact orientations and locations of the pigments. Finally, the time-resolved data are not easily interpreted because the system exhibits both multiexponential behavior and pronounced wavelength dependence.[1,12]

PSII has several structural and functional analogies with the better characterized and better understood photosynthetic reaction centers of purple bacteria. The bacterial reaction center (BRC) has been extensively investigated in both experimental and theoretical studies, enabled in part by the availability of several high-quality crystal structures, the ability to perform site-directed mutagenesis, and the development of ultrafast laser systems based on Ti/sapphire.

In contrast to that in the PSII, a semiquantitative understanding of the charge separation in the BRC is straightforward.[13] The electronic states of the BRC are well-separated and well-characterized. To the first order, decay constants in the exponential fits of time-resolved absorption or emission data can be assigned to physically distinct processes. The absorption of a photon results in ultrafast energy transfer to the lower excitonic state of the special pair, a strongly coupled bacteriochlorophyll dimer. The charge separation occurs on a time scale of 3 ps to form the P^+BPheo^- ion pair, where P^+ is a member of the special pair and BPheo is the bacteriopheophytin. Subsequent electron transfer on a 200−250-ps time scale results in the formation of the secondary $P^+Q_A^-$ ion pair, where Q_A^- is the reduced ubiquinone. The questions being addressed in studies of the charge separation in the BRC are increasingly more sophisticated, including a quantitative model for the ultrafast energy transfer[14] and investigations of the factors dictating unidirectional electron transfer and the role of specific amino acid side chains in the mediating electron transfer.[15−17]

Thus far, attempts to model PSII have relied on kinetic analyses using various data-fitting schemes.[1,7] However, it is problematic to draw connections between the fitting parameters and a physical interpretation of the energy-transfer and charge-transfer processes. A physical model of exciton−exciton coupling in the reaction-center core, the "multimer model", has been introduced and is consistent with some of the experimental data.[18,19] While this multimer model will explain some of the steady-state and early-time spectral data at low temperature and at room temperature, it does not include the effects of the charge separation and cannot describe the overall dynamics of the system.

In the present paper, we develop a dynamical model for PSII in which the parameters have a clearly assignable physical interpretation, many of which can be independently determined from other experiments. The data are not fit, globally or otherwise, to models consisting of sums of exponentials. In the context of this model, the population dynamics within the reaction-center complex are converted to spectroscopic observables so that the model can be compared with experimental results.

10.1021/jp021983k CCC: $25.00
Published on Web 02/08/2003

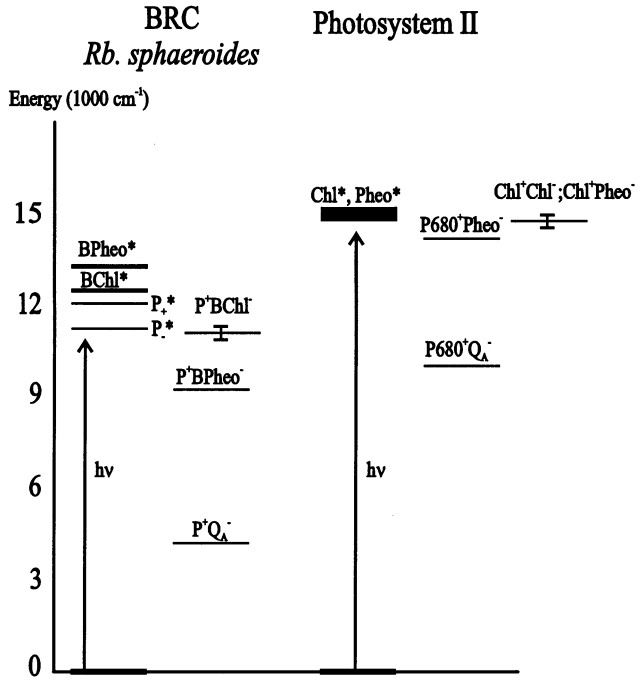

Figure 1. Schematic diagram of the energetics of BRC and PSII showing the exciton states (labeled with *) and charge-transfer states.

Our model begins with the observation that the descriptions of Frenkel exciton relaxation in a dissipative medium and adiabatic electron transfer in a dissipative medium have the same mathematical structure and can be treated on the same footing, as implied by Yokojima et al.[20] Furthermore, the action of the dissipative medium upon both the Frenkel excitonic and charge-transfer states should be similar because one of the primary mechanisms of electron-vibration coupling is polar solvation. Relaxation through a manifold of electronic states (obtained by considering both exciton and electron transfer) coupled to a dissipative medium is, in many respects, identical to the friction-induced relaxation of an anharmonic oscillator, which is known to yield multiexponential behavior.[21]

A second observation is that in PSII the typical interaction energies are all very similar in magnitude: exciton−exciton coupling (20−100 cm^{-1}),[18] typical tunneling energies calculated between pigments in reaction centers (10−150 cm^{-1}),[18,22,23] and the estimated driving forces for the charge-transfer steps (50−600 cm^{-1}).[24−26] This similarity is in sharp relief to the BRC systems in which these three energies span different ranges: 100−400, 10−150, and 400−2000 cm^{-1}, respectively.[25,27−30] The energetics of PSII and the BRC are compared schematically in Figure 1. These energetic differences lead to disparate dynamics for PSII and the BRC following photoexcitation. The resulting differences include the possibilities of rapid (<1 ps) charge transfer to an accessory chlorophyll and slower electron transfer to the pheophytin in PSII.

In this paper, we will focus primarily on the calculation of time-dependent fluorescence signals, although the methodology is readily extended to time-resolved transient-absorption experiments. The analysis of room-temperature transient-absorption measurements will be considered in a future publication.

II. The Model

We begin by choosing a convenient form for the Hamiltonian of the unperturbed electronic states. Because we wish to include the effects of energy transfer both through electromagnetic interactions (exciton exchange) and via tunneling interactions (charge transfer), it is necessary to adopt a representation that explicitly includes the positions of both the electron and hole. Thus, the basis states are represented as $|ij\rangle$, where i is the site index of the electron and j is the site of the hole. This representation has been used to describe excitons in finite solid systems.[20,31] States for which $i = j$ are excitonic in nature; the others all involve electrons and holes on different sites, that is, charge transfer. In principle there are n^2 such basis states to consider, where n is the number of sites, but in practice we only need to consider a small subset of these states because some configurations are prohibitively high in energy.

The Hamiltonian for the electronic states in the absence of the bath is given by

$$H = \sum_{ij} E_{ij}|ij\rangle\langle ij| + \sum_{ii,jj(ii\neq jj)} H^{\mathrm{ex}}_{ii,jj}|ii\rangle\langle jj| + \sum_{ij,il(j\neq l)} H^{\mathrm{ct}}_{ij,il}|ij\rangle\langle il| \quad (1)$$

where E_{ij} is the energy of each electron−hole configuration, H^{ex} are the off-diagonal terms that arise from excitonic coupling between sites, and H^{ct} are the off-diagonal terms that permit the transfer of an electron from one site to another. When the excitonic states are grouped together, the electronic Hamiltonian has the form

$$H = \begin{bmatrix} H^{\mathrm{ex}} & H^{\mathrm{ex,ct}} \\ H^{\mathrm{ex,ct}} & H^{\mathrm{ct}} \end{bmatrix} \quad (2)$$

This is the form used by Warshel and Parson to describe the special pair in the BRC.[32] In the case of PSII, however, all of the pigments must be considered simultaneously. This is a direct consequence of the fact that all of the couplings are comparable in magnitude and the site energies are similar. Thus, the separation of a "special pair" from the other pigments is not possible. This is the essence of the "multimer" model mentioned above[18] and a necessary component of any model of PSII.

The effects of the protein environment are represented as a bath of harmonic oscillators that are linearly coupled to each individual configuration of the electron and hole. The full system-bath Hamiltonian is

$$H = \sum_{ij} E_{ij}|ij\rangle\langle ij| + \sum_{ii,jj(ii\neq jj)} H^{\mathrm{ex}}_{ii,jj}|ii\rangle\langle jj| + \sum_{ij,il(j\neq l)} H^{\mathrm{ct}}_{ij,il}|ij\rangle\langle il| + \sum_{\alpha,ij} H^{\mathrm{HO}}_{\alpha} + \sum_{\alpha,ij} c_{\alpha,ij}Q_{\alpha}|ij\rangle\langle ij| \quad (3)$$

Here, H^{HO}_{α} is the harmonic-oscillator Hamiltonian for a given bath mode α:

$$H^{\mathrm{HO}}_{\alpha} = \frac{P_{\alpha}^{\,2}}{2m_{\alpha}} + \frac{1}{2}m_{\alpha}\omega_{\alpha}^{\,2}Q_{\alpha}^{\,2} \quad (4)$$

and $c_{\alpha,ij}$ is the coupling between the vibrations of the protein and the energy of a given electron−hole configuration. We assume for simplicity that all of the $c_{\alpha,ij}$'s are identical, that is, the lattice modulates the energy gap between the highest occupied and lowest unoccupied molecular orbitals of each pigment in the same manner. In the limit in which there are only two electronic states, this is the spin-boson Hamiltonian, which is discussed extensively in the literature.[33−35] Following this literature, we define the spectral-density function as

$$J(\omega) = \frac{\pi}{2}\sum_{\alpha}\frac{c_{\alpha,ij}^{\,2}}{m_{\alpha}\omega_{\alpha}}\delta(\omega - \omega_{\alpha}) \quad (5)$$

The spectral-density function, $J(\omega)$, is directly proportional to the population transition rate between any two electronic levels obtained using first-order perturbation theory (Fermi's golden rule). To obtain the transition rate for a given pair of energy eigenstates, we need to calculate the projection of each basis state on the electronic energy level using the eigenvectors of the electronic Hamiltonian and calculate the phonon occupancy of each bath mode. The final result for the transition rate from electronic state A to state B is[33,36]

$$R_{A,B} = J\left(\frac{|\epsilon|}{\hbar}\right)\frac{e^{-\beta\epsilon/2}}{\sinh\left(\frac{\beta|\epsilon|}{2}\right)}\sum_{ij}|\phi_{A,ij}|^2|\phi_{B,ij}|^2 \tag{6}$$

where $\beta = 1/k_bT$, $\varphi_{A,ij}$ is the amplitude of eigenstate A projected onto a particular electron−hole distribution ij, and $\epsilon = E_A - E_B$ is the energy difference between eigenstates A and B. The equation for R constitutes a master equation for the population dynamics within a reaction center, given by

$$\frac{dP_A(t)}{dt} = \sum_B R_{B,A}P_B(t) - \sum_B R_{A,B}P_A(t) \tag{7}$$

The master equation is solvable by the usual eigenvector methods used to solve coupled first-order differential equations: given an initial condition, $P(0)$, the populations are determined for all later times, $P(t)$. The master equation methodology has been applied to many similar problems that exhibit complicated dynamics, such as the vibrational relaxation of small molecules in solution,[37] excitonic processes in light-harvesting antennae,[36] and electron transfer in two-state systems.[33]

Although we have given a rather heuristic treatment, the same master equation can be derived from the application of Redfield theory combined with several approximations.[38,39] Coherent processes are not included; that is, we do not consider the evolution of the off-diagonal elements of the density matrix and, furthermore, assume that R has no elements that couple these terms to the diagonal population terms. This assumption requires that the correlation time of the bath be sufficiently short so that the electronic states are completely dephased before a significant population transfer occurs. These assumptions were previously employed by Kühn and Sundström to model the excitation-energy transfer in photosynthetic antenna complexes[36] and by Leegwater et al. to model exciton-relaxation processes in the proposed PSII multimer.[19] In addition, we assume that the tunneling matrix elements between pigments are sufficiently large so that the electron transfer is in the adiabatic limit.

The master-equation method yields the population of each state as a function of time. The next step is to relate these population changes to optical experiments, such as time-resolved fluorescence and pump−probe data. To do this, it is necessary to compute the transition dipole moment of each electronic state. Two assumptions are adopted: (1) the charge-transfer basis functions have no oscillator strength, and (2) the transition dipole moment of each individual pigment in the protein environment is that of the isolated pigment. Under these two assumptions, the transition dipole moment from the ground state to an electronic state, S, is given by

$$\vec{\mu}_S = \sum_{ii}\varphi_{S,ii}\vec{\mu}_{ii} \tag{8}$$

where $\varphi_{S,ii}$ is the amplitude of state S upon a given excitonic state ii. The sum extends only over the "excitonic" states (assumption 1), and the μ_{ii}'s are the individual pigment-transition moments (assumption 2) whose orientations are determined from a structural analysis of the protein.

Once the transition dipole moments are known, a stick spectrum of the reaction-center complex is generated according to eq 9. To generate a model absorption spectrum, the stick

$$I(\omega) = \sum_S \delta(\omega - \omega_S)|\vec{\mu}_S|^2 \tag{9}$$

spectrum is convolved with a line-shape function $G(\omega)$, which is assumed to be Gaussian, for convenience. The absorption band of a single transition is given by

$$A(\omega) = I_S(\omega) * G(\omega) \tag{10}$$

The definition of the absorption line shape also permits a calculation of the initial population distribution following optical excitation by a pulse with a spectral distribution $L_{pump}(\omega)$. The population of a specific state, S, following optical excitation is given by

$$P_S(0) = \int d\omega\, L_{pump}(\omega)\, A_S(\omega) \tag{11}$$

Once the initial populations, $P_S(0)$, are determined, the time-resolved magic-angle fluorescence spectrum is then given by

$$F_{MA}(t,\omega) = \sum_S A_S(\omega)\, P_S(t) \tag{12}$$

In the experimental work, the fluorescence emission is generally wavelength resolved so only a subset of the excited population distribution is probed. The ratio of the observed population of a state to its actual population at a given probe wavelength is given by $\zeta_S(t)$:

$$\zeta_S(t) = \frac{\int d\omega\, A_S(\omega)\, L_{probe}(\omega)\, P_S(t)}{\int d\omega\, A_S(\omega)} \tag{13}$$

Here, $L_{probe}(\omega)$ is the band pass of the optical filter, assumed to be a Gaussian function. The time-resolved fluorescence signal, measured at the magic angle following optical excitation from the ground state, is then given by

$$Fl_{MA}(t) = \sum_S \zeta_S(t) \tag{14}$$

In summary, our methodology combines three models to calculate the time-dependent spectroscopic behavior. The necessary components are (1) a model of the electronic states of the pigment array, (2) a model for the interaction of the protein with the electronic states, and (3) a model for the pigment orientation. In the following section, we present a scheme for obtaining the estimates of these parameters from results in the literature.

III. Pigment and Protein Parameters for PSII and the BRC

Electronic States. The first step in the development of an effective Hamiltonian for the electronic states of the reaction-center complex is to estimate the energies of each configuration in the electron−hole representation. While in principle there are n^2 configurations, where n is the number of sites (e.g., for

TABLE 1: Relative Diagonal Energies (cm^{-1})

	site distribution #1[a]	site distribution #2[b]
$Pheo_2$	0	−57
Chl_2	0	37
$P680_2$	0	8
$P680_1$	0	8
Chl_1	0	−67
$Pheo_1$	0	−173
Chl_1(antenna)	150	107
Chl_2(antenna)	150	171
$P680^+P680^-$	1850	
$P680^+Chl^-$	−125	
$P680^+Pheo^-$	−825	

[a] All core pigments are considered isoenergetic as in work by Durrant et al.[18] The two antenna chlorophyll are placed on the blue side of the absorption band. [b] Site energies for core and antenna pigments assigned along the lines of Parameter Set I deduced by Konermann and Holzwarth.[46]

BRC 36 "parameters"), in practice there are many configurations that are never observed experimentally for energetic or other reasons and thus may be "pruned" from the basis set. For example, it is not necessary to include configurations that place a cation on the pheophytin. The states are chosen in the following manner. All excitonic states are included, that is, those states that have the form $|ii\rangle$. The excitonic states all lie relatively close to one another, and the energies of these states are determined through an analysis of the structural and linear spectroscopic properties of the reaction center. In this study, two different sets of site energies have been used to represent the diagonal energies of the individual pigment Q_y transitions in PSII (Table 1). The calculations performed with each of the sets of site energies are compared and discussed below. The electronic-site energies are subject to static disorder or the random variation in the energy of each pigment due to its specific location in the protein environment. This disorder is taken into account by randomly selecting the energy for each diagonal element from a Gaussian distribution centered at the given site energy. For a given reaction center, the static disorder of each electronic state is independently selected. Typically, an ensemble of 150 reaction centers is calculated, and the results are averaged to obtain the inhomogeneously broadened result.

The charge-transfer states that are considered in the model are $|P680_{1(2)}^-P680_{1(2)}^+\rangle$, $|P680_{1(2)}^+Chl_{1(2)}^-\rangle$, and $|P680_{1(2)}^+Pheo_{1(2)}^-\rangle$ for PSII and $|P_{M(L)}^-P_{L(M)}^+\rangle$, $|P_{L(M)}^+Chl_{L(M)}^-\rangle$, and $|P_{L(M)}^+Pheo_{L(M)}^-\rangle$ for the BRC. P680 is one of the pigments analogous to the "special pair" in the BRC, which is believed to be the site of the oxidized chlorophyll. Chl^- is the reduced accessory chlorophyll that bridges the space between the P680 pigments and the pheophytins. $Pheo^-$ is the reduced pheophytin. The subscripts denote either the D1 branch or the D2 branch (analogous to the L and M subunits of the BRC, respectively). For the BRC, the state energies (relative to the photon energy) are 2500 cm^{-1} for $|P_{M(L)}^-P_{L(M)}^+\rangle$, −1000 cm^{-1} for $|P_{L(M)}^+Chl_{L(M)}^-\rangle$, and −2300 cm^{-1} for $|P_{L(M)}^+Pheo_{L(M)}^-\rangle$. The energy for $|P_{M(L)}^-P_{L(M)}^+\rangle$ is based on the calculations in ref 25. After transformation to the exciton basis, the intermediate states (with primary contributions from $|P_{L(M)}^+Chl_{L(M)}^-\rangle$) are ∼50 cm^{-1} below the lower exciton state associated with the special pair (P*), in keeping with the very small reaction energy estimated for this step.[25] The energy of the final state ($|P_{L(M)}^+Pheo_{L(M)}^-\rangle$) relative to P* is −1250 cm^{-1}, in accordance with experimental estimates ranging from −700 to −2000 cm^{-1}.[28−30] The sensitivity of the model to the value of this fitting parameter is detailed in the Results section.

TABLE 2: Off-Diagonal Matrix Elements

	$Pheo_2$	Chl_2	$P680_2$	$P680_1$	Chl_1	$Pheo_1$	Chl_1(ant)	Chl_2(ant)
$Pheo_2$		86.3	17.3	−1.2	−5.7	2.7	0	3
Chl_2	86.3		−101	−42.7	15.8	−5.5	0	0.5
$P680_2$	17.3	−101		120	−37.9	−1.7	1.5	0.5
$P680_1$	−1.2	−42.7	120		−90.2	17.2	3.5	0
Chl_1	−5.7	15.8	−37.9	−90.2		82.3	3.5	0
$Pheo_1$	2.7	−5.5	−1.7	17.2	82.3		7	0
Chl_1(ant)	0	0	1.5	3.5	3.5	7		0
Chl_2(ant)	3	0.5	0.5	0	0	0	0	

	$P680_2$	$P680_1$	$P680^+Chl_2^-$	$P680^+Chl_1^-$
$P680^+P680^-$	30	30	0	0
$P680^+Chl_2^-$	15	0	0	0
$P680^+Chl_1^-$	0	22	0	0
$P680^+Pheo_2^-$	0	0	64	0
$P680^+Pheo_1^-$	0	0	0	80

There are no experimental determinations of the comparable charge-transfer energetics in PSII, although relative energies for the final state, $|P680_{1(2)}^+Pheo_{1(2)}^-\rangle$, have been estimated in recombination studies to be from −160 to > −950 cm^{-1}.[24,26,40,41] These values are much more negative than the negligible stabilization energies predicted by quantum calculations.[25] In the present model, this is an adjustable parameter; we found that the value −825 cm^{-1}, within the range suggested by the experimental models, gives acceptable results. A nearly zero value, suggested by the quantum model, results in virtually no charge separation, and a magnitude significantly smaller than −800 cm^{-1} results in little charge separation. The energy of the state $|P680_{1(2)}^-P680_{1(2)}^+\rangle$ is estimated on the basis of the calculated values of the ionization potential and electron affinity for P680 in ref 25.

Having established the diagonal elements of the Hamiltonian, the next step is to determine the off-diagonal elements. Given the positions, orientations, and site energies for the pigments in the reaction-center complex, the off-diagonal elements may be estimated as the dipole−dipole interaction matrix elements. The approximation that the pigments can be considered point dipoles is qualitatively but not quantitatively accurate, given the close proximity of the pigments in the reaction center. In addition, Dexter-type exchange terms may be important if the pigments are in van der Waals contact. For the BRC, we use the off-diagonal matrix elements obtained by Won and Friesner for exciton coupling,[27] and for PSII, we use the "multimer" values of Durrant et al.[18]

The other off-diagonal terms in the Hamiltonian represent the tunneling of electrons from one pigment to another. In the BRC literature, the values of these matrix elements range from 20 to 30 cm^{-1} for the electron transfer from P to BChl and about six times that for the electron transfer from BChl to BPheo.[22,23] In the BRC model, we used the couplings reported by Zhang and Friesner[22] with one exception. The $BChl_M$ to $BPheo_M$ coupling was reduced from 95 to 30 cm^{-1}, effectively inactivating the M branch so that the model is consistent with the behavior of wild-type reaction centers. In our calculations for PSII, the charge-transfer couplings are treated as fitting parameters but the values chosen are consistent with the literature estimates. On the basis of the suspected structural similarities between PSII and other structurally solved reaction centers,[42] the tunneling matrix elements should also be about 20−30 cm^{-1} between the P680 and Chl sites. Our values for this pruned Hamiltonian for PSII are presented in Tables 1 and 2.

Protein Vibrational Modes. The spectral-density function represents the influence of the protein modes on the electronic

TABLE 3: Transition-Dipole Matrix Elements (Normalized to 1 for Chlorophyll and 0.8 for Pheophytin)

	$Pheo_2$	Chl_2	$P680_2$	$P680_1$	Chl_1	$Pheo_1$
x	0.616 617	−0.913 473	0.643 991	−0.963 994	0.460 165	0.157 352
y	0.498 634	0.316 914	−0.716 394	0.239 023	−0.887 812	0.533 105
z	0.066 872	0.255 210	0.268 432	0.116 548	0.006 159	−0.569 539

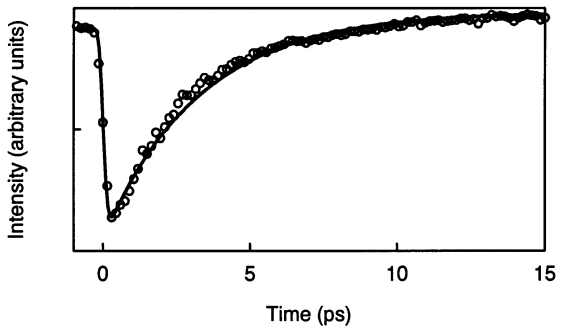

Figure 2. Time-resolved emission profiles of the BRC: model calculation (solid line) and experimental data (points) from *Rb. sphaeroides* reaction centers, with an 860-nm excitation and 940-nm probe (data from ref 44). In the calculation, the relative energy of the final state is -1250 cm^{-1} with $\omega_c = 550$ cm^{-1} and $\eta = 1.1$.

states of the pigments. For a large protein bath, the spectral density can be estimated as a continuous "ohmic" function:[33]

$$J(\omega) = \eta\omega \exp(-\omega/\omega_c) \tag{15}$$

Here η is a "friction" and ω_c is a "cutoff" frequency for the bath. The shape of the spectrum is controlled by a single parameter, ω_c, which is partially constrained by the results of the molecular dynamics simulations, low-temperature hole-burning results, fluorescence line-narrowing experiments (FLN), and the requirement that there is sufficient spectral density to permit transitions between all the different electronic states of the systems, which are accessible through vibrational transitions. These constraints are not always completely compatible. For example, in the bacterial light-harvesting antennae, low-temperature hole-burning results determine ω_c to be $\sim$110 cm^{-1},[39] but fits of the molecular dynamics calculations of electron transfer in the BRC indicate a value closer to 500 cm^{-1}.[23] The difference between these two estimates of ω_c arises from the fact that the hole-burning and fluorescence experiments typically reveal only the contribution of the protein mode in calculating ω_c. For electron-transfer calculations, it is necessary to consider both the "phonon" spectrum of the protein and the intramolecular vibrations of the pigments because both modulate the electronic energy level. In PSII, hole-burning[5] and FLN[3] experiments suggest small values for ω_c ($\sim$20 cm^{-1}) but also indicate that there are substantial contributions from the higher frequency modes. Thus, setting ω_c to be $\sim$150 cm^{-1}, which gives acceptable results in our model, is a reasonable compromise between the values derived from the molecular dynamics calculations and hole-burning and FLN experiments; it represents an "average" value of the phonon frequency.

Once ω_c is established, η for the overall reaction P−Pheo → P^+Pheo^- is constrained by the need to make the reorganization energy of the three-state system, which is given by[33,39]

$$\lambda = 4\frac{\hbar}{\pi}\int\frac{J(\omega)}{\omega}\,d\omega \tag{16}$$

match the driving force. This constraint is imposed to be consistent with the experimental results that suggest that the classical activation energy is small (compared to that at room temperature).[4] This constraint is not absolute, however, and our formulation of the problem involves many different transitions and not just a single step. In principle, each possible state-to-state transition should have its own value of η. Given the approximation of the spectral density, this level of detail is clearly not justified and we use only a single value of η. In this view, η, like ω_c, represents an average value for the strength of the interaction between the vibrational modes of the proteins and pigments and the electronic states of the system. Typical values of η obtained from the fit of the model to the data for this system are approximately unity (vide infra).

Pigment Orientations. To calculate the absorption and fluorescence spectra, a model for the pigment orientations is required. For the BRC, the relative orientations of the pigments are well defined by the known crystal structures. In the case of PSII, the exact pigment orientations are not known from the available structural analyses. We follow the common assumption that the relative orientations of the pigments are similar to the BRC. In these initial calculations, the two antenna chlorophyll are assumed to have orientations parallel to the nearest pheophytin molecules. This assumption is roughly consistent with the recent 3.8-Å crystal structure of PSII,[11] which resolves the pigment planes but not the dipole orientations. Table 3 contains the normalized transition dipoles for the six pigments of the reaction center used in the present calculation.[27] The spectra were simulated with a homogeneous Gaussian line width of 200 cm^{-1} [full width at half-maximum (fwhm)], as suggested by Cattaneo et al. in their thermal broadening analysis of the spectrum.[43]

IV. Results

BRC. The kinetics of charge transfer in the BRC were calculated in order to test the applicability of the model on a well-known system. In Figure 2, the calculated fluorescence is plotted as a function of time along with the experimental data.[44] The simple exponential formation of the final state has a time constant of $\sim$3 ps, which is consistent with the experimental results. As described above, the main fitting parameter is the energy of the final state $|P_{L(M)}^+Pheo_{L(M)}^-\rangle$ relative to P*. To test the robustness of the model, this relative energy was varied from -700 to -2000 cm^{-1} and the reorganization energy (controlled by ω_c) was adjusted accordingly. The resulting time constants for the formation of the final state ranged from $\sim$1 to $\sim$5 ps. The best agreement with the *Rhodobacter sphaeroides* experimental data shown in Figure 2 was obtained with a relative energy of -1250 cm^{-1}. These results show that the model is fairly robust with respect to the uncertainty of the main fitting parameters.

PSII. Fluorescence kinetics were calculated for different pump and probe wavelengths between 660 and 690 nm. The calculated fluorescence profiles were convolved with the appropriate instrument-response function to compare them with the previously reported experimental data.[45] The model result for site distribution #1, with the six main reaction-center pigment transitions all at the same energy (Table 1), is shown with the experimental data in Figure 3. The model is able to capture the major features of the experimental results, including the 20−40- and $\sim$200-ps decay components. This good agreement was obtained by adjusting the bath coupling strength and the Chl−

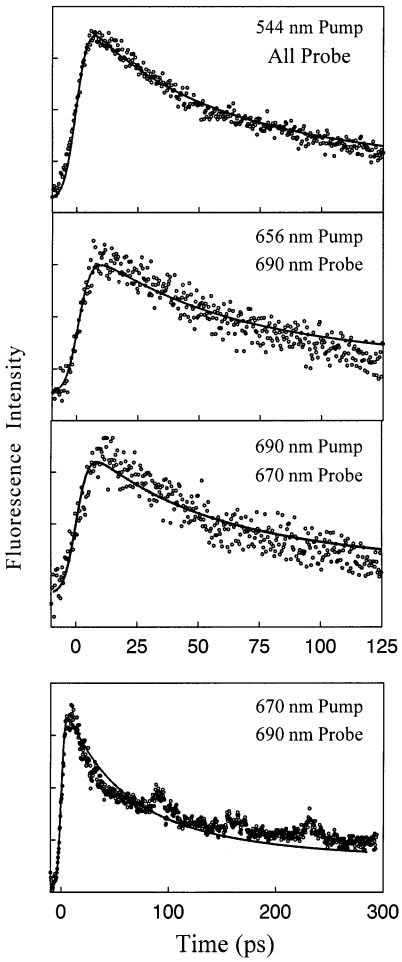

Figure 3. Time-resolved fluorescence profiles of PSII: model calculation (solid line) and experimental data from ref 45 (points). In the topmost plot, the 544-nm pump effectively excites all of the chromophores and the total fluorescence emission is monitored. The discontinuities in the 670-nm-pump/690-nm-probe experimental data set at ~90, ~170, and ~240 ps are instrumental artifacts.

Pheo tunneling matrix elements within a range justified by the available literature values. These two sets of parameters tend to compensate for each other, so several combinations were found to give equally good fits to the experimental data (based on χ^2 analyses). The values shown in Table 2 are characteristic of the middle of the fitting range and were found to give the best fit with $\omega_c = 150$ cm^{-1} and $\eta = 1$. The relative energies of the charge-separated states were generally held fixed. When the energy difference of the final state was increased, η and ω_c also increased and compensated for the change to give comparable fits (e.g., for $\Delta E = -925$ cm^{-1}, $\omega_c = 170$ cm^{-1}, and $\eta = 1.1$). The minimum energy difference that still produced a good fit was $\Delta E = -725$ cm^{-1}, with $\omega_c = 140$ cm^{-1} and $\eta = 0.8$.

Site distribution #1, with isoenergetic pigment transitions, is a convenient approximation, often used, and justified by the fact that the transitions overlap spectrally. It is unlikely, however, that the site energies are precisely identical in the PSII reaction center. The second set of site energies tests how the model behaves with a more realistic distribution, that is, with the pigments having different transition-site energies. Site distribution #2 (Table 1) is based on Konermann and Holzwarth's decomposition of the reaction-center absorption spectra at different temperatures and pigment contents.[46] Even though their analysis is based on assumptions different from those of the present model (e.g., no excitonic coupling), their parameters can provide a starting point for assigning diagonal energies. In our model, neither of their proposed parameter sets gives a good fit to the room-temperature spectrum. However, exchanging the assignment of an accessory Chl with that of an antenna Chl in Konermann and Holzwarth's Parameter Set I so that both antennae are on the blue side of the spectrum[47] does give a good fit to the spectrum, as shown in Figure 4. The model yields comparable spectra given the two different site distributions due to the width of the homogeneous and inhomogeneous broadening, which are comparable to the shifts in the diagonal site energies.

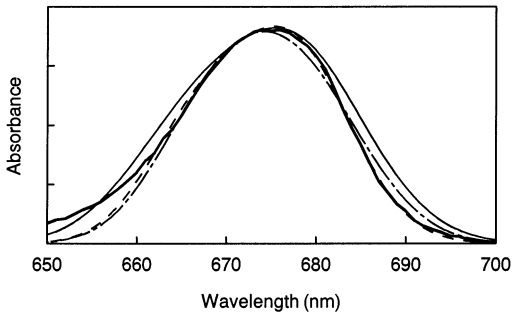

Figure 4. PSII absorption spectra. The experimental data (thick solid line) are compared with the model calculations from site distribution #1 (dashed line) and site distribution #2 (dot−dashed line). The spectrum calculated with an inhomogeneous broadening of 210 cm^{-1} (fwhm) is shown with a narrow solid line.

The calculated fluorescence profiles for site distribution #2 are comparable to those shown in Figure 3 for site distribution #1, although adjustments to the protein-bath coupling parameters were necessary to obtain the same goodness of fit. Specifically, ω_c increased to 155 cm^{-1} and η increased to 1.3. The only difference observed in the calculated kinetics between the two site distributions is in the initial fast component. The importance of this initial fast component was discussed in our previous paper:[45] each experimental fluorescence trace exhibits an instrument-limited rise, except for the 690-nm-pump/670-nm-probe data set. The rise in this fluorescence is thought to be limited by slow energy transfer from the red-absorbing pigments to the blue-emitting pigments. The present model also predicts a slower rise for the 690-nm-pump/670-nm-probe wavelength combination, although the calculated rise-time constant is shorter than that determined experimentally. Site distributions #1 and 2 have rise components of ~1.5 and ~3 ps, respectively, while the analysis of the experimental data reveals the rise component to be ~6−8 ps.[45] For a given site distribution, the calculated rise component can be controlled by changing the energy-transfer matrix elements that couple the antenna pigments to the core of the reaction center. Decreasing the coupling effectively slows down the energy transfer between the antenna pigments and the reaction center and increases the calculated rise-time constant. When the couplings are decreased to <7 cm^{-1}, no further improvement is obtained.

V. Discussion

We have developed a model for the energy-transfer and charge-transfer dynamics in PSII that is able to describe both the absorption spectrum and the overall characteristics of the time-resolved fluorescence using physically meaningful parameters. This is an improvement over models that attempt to assign meaning to multiple exponential-fitting parameters. The model also successfully fits the charge-transfer kinetics for the better-known BRC. The input parameters were deduced directly from

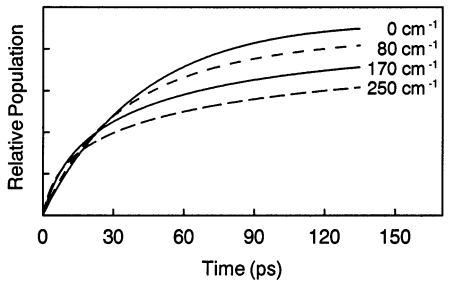

Figure 5. Calculated population kinetics of the $P680^+Pheo^-$ radical pair with an inhomogeneous broadening from 0 to 250 cm^{-1} (fwhm).

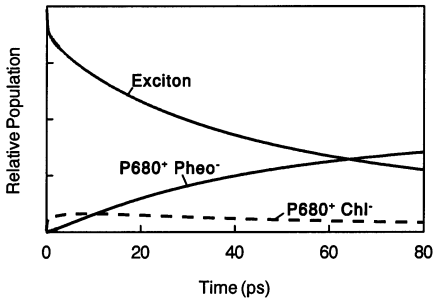

Figure 6. Calculated population kinetics of the charge separation in PSII following 660-nm excitation. The radical populations shown are for the D1 branch.

independent experimental studies or were estimated from a range constrained by the experimental results. It should be noted that, although some inputs were treated as fitting parameters, the range of the fitting space is limited by the thermodynamic constraints of the system, the parameters could not freely float, and overall the model is robust.

Inhomogeneous Broadening. Both homogeneous and inhomogeneous broadening make significant contributions to the spectral line width of PSII reaction centers at room temperature. Our random site-energy distribution, 90 cm^{-1} fwhm, is narrower than that used by Durrant et al. in their multimer model (210 cm^{-1} fwhm).[18] In our simulations, the absorption spectrum calculated with an inhomogeneous site-energy broadening of 210 cm^{-1} was in poor agreement with the experimental data (see Figure 4), although better agreement could be obtained by decreasing the homogeneous broadening. However, this adjustment would be contrary to the spectral evidence that at room temperature the broadening is dominated by the homogeneous component.[43,46] Following these references, we use 90 cm^{-1} for the inhomogeneous component and 200 cm^{-1} for the homogeneous component.

The inhomogeneous broadening has an important influence on the calculated kinetics as well as on the spectrum. To investigate the effect on the kinetics, the model was run without any static disorder. Two main consequences were evident. The first effect is in the formation of the final charge-separated state $|P680_{1(2)}^+Pheo_{1(2)}^-\rangle$. The yield of this state decreases as the disorder increases, as shown in Figure 5. With increasing disorder, the coupling between the pigments in a fraction of the distribution of reaction centers is weakened, so the charge transfer is inhibited. The same effect has been observed experimentally in damaged reaction centers.[24] In the absence of broadening, the population rises with a simple exponential function. The broadened result is characterized by a slightly faster rise and a slower long component. The corresponding shape of the calculated fluorescence trace is very sensitive to the degree of static disorder, and values greater than $\sim$100 cm^{-1} (fwhm) are unable to fit the experimental data. All excitation wavelengths show the same trend. This multiexponential behavior originating from static disorder has been observed in other studies of PSII.

In addition, the energy transfer between the red and blue pigments slows down. In the broadened case, time constants of 1.5−3 ps were calculated; in the absence of broadening, the time constants increase to 2.5−6 ps. Even though this brings the model into better agreement with the experimental data (time constants of 6−8 ps), it is not likely the source of disparity because the complete absence of static disorder is an unrealistic assumption. Yang and Fleming[48] recently introduced a more refined model for the static disorder that may have some bearing here. In their model, a given reaction center has a small degree of disorder between the individual pigments but all the pigments of that reaction center have a common static shift relative to the other reaction centers of the ensemble. With this two-dimensional approach, it may be possible to refine our present model.

Energy Transfer in the Reaction Center. An important experimental finding is that the fluorescence at 670 nm following excitation at 690 nm has a slower rise time than the other wavelength combinations. The model predicts this effect qualitatively but not quantitatively. As stated above, the calculated rise-time constants are $\sim$1.5−3 ps, while the experiments show a rise of $\sim$6−8 ps. Of note is the difference between the site distributions: the time constant is significantly slower for site distribution #2. A possible route to obtaining better quantitative fits may involve adjusting the site energies accordingly. However, the current data are not adequate to determine a unique "best" site distribution.

As discussed above, the slow rise in the blue fluorescence following red excitation results from the weak coupling between the antenna pigments and the rest of the reaction center. The model predicts the same slow rise for the opposite situation: red fluorescence following blue excitation. This contrasts with the experimental result in which the rise in the red fluorescence is fast (instrument-limited). There are several possible explanations for this discrepancy. The first lies in the model assumption that all pigments have the same symmetric line width. In reality, the homogeneous widths of the red bands, primarily P680, are thought to be much broader than those of the blue bands[43] and skewed toward the blue side of the spectrum.[46] In addition, the vibronic structure of each electronic state extends toward higher energy. Thus, in the experiments (but not in the model), excitation in the blue would also excite the high-energy wing of the red-pigment absorption bands, allowing them to fluoresce promptly before the longer-time-scale energy transfer is complete.

Implications of the Model. To the extent that this model represents the actual energy-transfer and charge-transfer dynamics of PSII, we can examine the predicted subpicosecond dynamics, even though comparable fluorescence data at this resolution are still not available. The calculated radical populations at short times are shown in Figure 6 for 660-nm excitation. The other excitation wavelengths show the same qualitative behavior. The $P680^+Chl^-$ radical pair is calculated to form on a fast time scale, reaching a nearly steady state on the order of a picosecond, depending on the excitation wavelength. The formation of $P680^+Pheo^-$ is calculated to follow with a time constant of approximately 35−50 ps. The model results lend support to the idea of an ultrafast component of the charge separation for the $P680^+Chl^-$ radical pair, but not the $P680^+Pheo^-$ pair. The calculated wavelength dependence of the initial fast step is shown in Figure 7. The charge separation occurs nearly

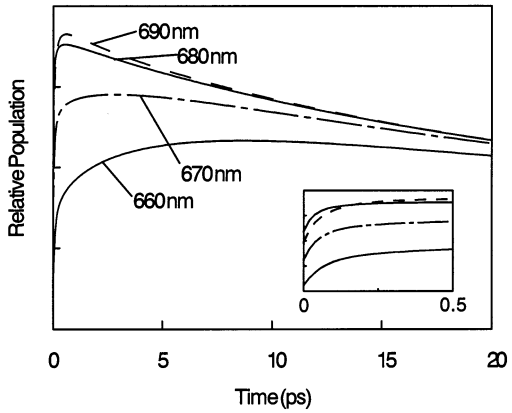

Figure 7. Calculated population kinetics of the $P680^+Chl^-$ radical pair from different excitation wavelengths.

instantaneously after excitation of P680 and the other red-absorbing pigments. When the blue pigments are pumped, the charge separation occurs after the slower energy transfer to the red states.

The model predictions of radical populations are based on our assumption of a single charge-transfer pathway, namely that P680 initially donates an electron to Chl followed by an electron transfer to Pheo. This is probably an oversimplification of the mechanism, given the likelihood of alternative charge-transfer pathways found in the BRC.[13] Recently, Prokhorenko and Holzwarth reported evidence that in PSII at low temperatures the initial electron donor is the accessory chlorophyll, so that the mechanism proceeds through Chl^+Pheo^- to the final $P680^+Pheo^-$ radical pair.[9] Incorporation of these or other charge-transfer states into the model would alter the predicted kinetics, especially at short times where experimental data are not available; however, the current experimental data do not justify this step. As more detailed experimental data become available at shorter time resolutions (e.g., from fluorescence upconversion), the validity of these calculations can be tested and further refinements to the model will be possible.

Acknowledgment. This work is supported by NSF MCB-9727948. J.J.S. was supported in part by the Center for Ultrafast Optical Science NSF STC PHY 8920108.

References and Notes

(1) Gatzen, G.; Muller, M. G.; Greibenow, K.; Holzwarth, A. R. *J. Phys. Chem.* **1996**, *100*, 7269.
(2) Greenfield, S. R.; Seibert, M.; Govindjee; Wasielewski, M. R. *J. Phys. Chem. B* **1997**, *101*, 2251.
(3) Peterman, E. J. G.; van Amerongen, H.; van Grondelle, R.; Dekker, J. P. *Proc. Natl. Acad. Sci. U.S.A.* **1998**, *95*, 6128.
(4) Groot, M.-L.; van Mourik, F.; Eijckelhoff, C.; van Stokkum, I. H. M.; Dekker, J. P.; van Grondelle, R. *Proc. Natl. Acad. Sci. U.S.A.* **1997**, *94*, 4389.
(5) Jankowiak, R.; Ratsep, M.; Picorel, R.; Seibert, M.; Small, G. J. *J. Phys. Chem. B* **1999**, *103*, 9759.
(6) Greenfield, S. R.; Seibert, M.; Govindjee; Wasielewski, M. R. *J. Phys. Chem. B* **1999**, *103*, 8364.
(7) Konermann, L.; Gatzen, G.; Holzwarth, A. R. *J. Phys. Chem. B* **1997**, *101*, 2933.
(8) Johnston, H. G.; Wang, J.; Ruffle, S.; Sayre, R. T.; Gustafson, T. L. *J. Phys. Chem. B* **2000**, *104*, 4777.
(9) Prokhorenko, V. I.; Holzwarth, A. R. *J. Phys. Chem. B* **2000**, *104*, 11563.
(10) Barter, L. M. C.; Bianchietti, M.; Jeans, C.; Schilstra, M. J.; Hankamer, B.; Diner, B. A.; Barber, J.; Durrant, J. R.; Klug, D. R. *Biochemistry* **2001**, *40*, 4026.
(11) Zouni, A.; Witt, H.-T.; Kern, J.; Fromme, P.; Krauss, N.; Saenger, W.; Orth, P. *Nature* **2001**, *409*, 739.
(12) Konermann, L.; Yruela, I.; Holzwarth, A. R. *Biochemistry* **1997**, *36*, 7498.
(13) van Brederode, M. E.; van Grondelle, R. *FEBS Lett.* **1999**, *455*, 1.
(14) Jordanides, X. J.; Scholes, G. D.; Fleming, G. R. *J. Phys. Chem. B* **2001**, *105*, 1652.
(15) Kirmaier, C.; Weems, D.; Holten, D. *Biochemistry* **1999**, *38*, 11516.
(16) Ivashin, N.; Källebring, B.; Larsson, S.; Hansson, Ö. *J. Phys. Chem. B* **1998**, *102*, 5017.
(17) Pudlak, M.; Pincak, R. *Chem. Phys. Lett.* **2001**, *342*, 587.
(18) Durrant, J. R.; Klug, D. R.; Kwa, S. L. S.; van Grondelle, R.; Porter, G.; Dekker, J. P. *Proc. Natl. Acad. Sci. U.S.A.* **1995**, *92*, 4798.
(19) Leegwater, J. A.; Durrant, J. R.; Klug, D. R. *J. Phys. Chem. B* **1997**, *101*, 7205.
(20) Yokojima, S.; Meier, T.; Mukamel, S. *J. Chem. Phys.* **1997**, *106*, 3837.
(21) Shiang, J. J.; Liu, H.; Sension, R. J. *J. Chem. Phys.* **1998**, *109*, 9494.
(22) Zhang, L. Y.; Friesner, R. A. *Proc. Natl. Acad. Sci. U.S.A.* **1998**, *95*, 13603.
(23) Makri, N.; Sim, E.; Makarov, D. E.; Topaler, M. *Proc. Natl. Acad. Sci. U.S.A.* **1996**, *93*, 3926.
(24) Booth, P. J.; Crystall, B.; Giorgi, L. B.; Barber, J.; Klug, D. R.; Porter, G. *Biochim. Biophys. Acta* **1990**, *1016*, 141.
(25) Blomberg, M. R. A.; Siegbahn, P. E. M.; Babcock, G. T. *J. Am. Chem. Soc.* **1998**, *120*, 8812.
(26) Groot, M.-L.; Peterman, E. J. G.; van Kan, P. J. M.; van Stokkum, I. H. M.; Dekker, J. P.; van Grondelle, R. *Biophys. J.* **1994**, *67*, 318.
(27) Won, Y.; Friesner, R. A. *J. Phys. Chem.* **1988**, *92*, 2208.
(28) Ogrodnik, A.; Keupp, W.; Volk, M.; Aumeier, G.; Michel-Beyerle, M. E. *J. Phys. Chem.* **1994**, *98*, 3432.
(29) Peloquin, J. M.; Williams, J. C.; Lin, X.; Alden, R. G.; Taguchi, A. K. W.; Allen, J. P.; Woodbury, N. W. *Biochemistry* **1994**, *33*, 8089.
(30) Holzwarth, A. R.; Muller, M. G. *Biochemistry* **1996**, *35*, 11820.
(31) Hill, N.; Whaley, K. B. *Chem. Phys.* **1996**, *210*, 117.
(32) Warshel, A.; Parson, W. W. *J. Am. Chem. Soc.* **1987**, *109*, 6143.
(33) Leggett, A. J.; Chakravarty, S.; Dorsey, A. T.; Fisher, M. P. A.; Garg, A.; Zwerger, W. *Rev. Mod. Phys.* **1987**, *59*, 1.
(34) Xu, D.; Schulten, K. *Chem. Phys.* **1994**, *182*, 91.
(35) Schulten, K.; Tesch, M. *Chem. Phys.* **1991**, *158*, 421.
(36) Kühn, O.; Sundström, V. *J. Chem. Phys.* **1997**, *107*, 4154.
(37) Liu, H. J.; Pullen, S. H.; Walker, L. A.; Sension, R. J. *J. Chem. Phys.* **1998**, *108*, 4992.
(38) Makri, N.; Makarov, D. E. *J. Chem. Phys.* **1995**, *102*, 4600.
(39) Egger, R.; Mak, C. H. *J. Phys. Chem.* **1994**, *98*, 9903.
(40) Volk, M.; Gilbert, M.; Rousseau, G.; Richter, M.; Ogrodnik, A.; Michel-Beyerle, M.-E. *FEBS Lett.* **1993**, *336*, 357.
(41) Roelofs, T. A.; Gilbert, M.; Shuvalov, V. A.; Holzwarth, A. R. *Biochim. Biophys. Acta* **1991**, *1060*, 237.
(42) Svensson, B.; Etchebest, C.; Tuffery, P.; vanKan, P.; Smith, J.; Styring, S. *Biochemistry* **1996**, *35*, 14486.
(43) Cattaneo, R.; Zucchelli, G.; Garlaschi, F. M.; Finzi, L.; Jennings, R. C. *Biochemistry* **1995**, *34*, 15267.
(44) Moser, C.; Sension, R. J.; Szarka, A. Z.; Repinec, S. T.; Hochstrasser, R. M.; Dutton, P. L. *Chem. Phys.* **1995**, *197*, 343.
(45) Donovan, B.; Walker, L. A., II; Kaplan, D.; Bouvier, M.; Yocum, C. F.; Sension, R. J. *J. Phys. Chem. B* **1997**, *101*, 5232.
(46) Konermann, L.; Holzwarth, A. R. *Biochemistry* **1996**, *35*, 829.
(47) Dekker, J. P.; Van Grondelle, R. *Photosynth. Res.* **2000**, *63*, 195.
(48) Yang, M.; Fleming, G. R. *J. Chem. Phys.* **2000**, *113*, 2823.